S. Hager*, H. Oesinghaus*, A. Bachmann, M. Meinardus, T. Hofmann, R. Engelbrecht and K. Glas

$CaCO_3$ deposits in reverse osmosis: Part III – Incipient Scaling detection via polymer optical fibre sensors. Comparison to hydrochemical prediction and image analytical methods

Reverse Osmosis (RO) is a widely used technology for water treatment in the beverage industry to produce brewing water, process water or tap water. The weak points of RO-membrane filtration are membrane degradation due to oxidative water constituents or membrane fouling in the difficult-to-clean, spacer-filled feed channel. The fouling can be distinguished into two main categories. The first one is caused by feed waters with a high organic and microbial load. The second type of fouling is triggered by supersaturated salt solutions, which leads to the precipitation of salts on the membrane surface. Both fouling types are destroying spiral wound RO-modules if they are not detected in an early stage. This work presents and validates a new optical online detection method via polymer optical fibres (POF) for inorganic fouling as $CaCO_3$, $CaSO_4$, $BaSO_4$, $SrSO_4$. The new detection method is tested by three experimental set-ups and compared with common prediction and detection methods such as saturation calculation, measurement of salt rejection, permeability, and the pressure drop in the feed channel. In addition to conventional online analysis methods for detecting deposits in reverse osmosis systems, this study presents an image analysis method that provides reliable evidence of POF sensor operation. The POF sensor is able to detect incipient crystal formation during the RO process. This gives this study the opportunity to discuss current crystallisation theories such as the induction time theory and the role of monohydrated calcium carbonate (MCC) as a precursor in the formation of $CaCO_3$ deposits.

Descriptors: reverse osmosis, scaling, polymer optical fibre sensors, image analysis, hydrochemical prediction, predictive maintenance

1 Introduction

With the widespread application of reverse osmosis (RO) to the treatment of a great variety of waters, the topic of membrane scaling became a subject of high research interest. In the 1980s, for example, numerous publications already deal with the avoidance of scaling on RO membrane modules [17]. Efficient RO operation and the associated challenges related to mineral deposits in membrane modules are drivers of a continued high level of research interest [10]. The findings of experimental scaling research are based on a great variety of methods for detecting crystals or their effect on the membrane process. In a recent study, for example, it is shown by transmission electron microscopy that $CaCO_3$ crystals of a few nm in size can be found in cavities of the microstructured polyamide surface that serves as the active RO membrane layer [19]. Research on the structure of already advanced salt deposition also provides important findings. For example, it has recently been shown by evaluating membrane permeability and subsequent ex-situ membrane analysis that an electromagnetic field (EMF) can be used to cause a permeability-improving change in crystal or scaling structure. The cleanability of the membrane surface could also be improved by applying the EMF. Energy dispersive X-ray spectroscopy (EDX) and scanning electron microscope (SEM) are used to analyse the scaling structure [11]. In another study it could be shown that a permeability decrease of the membrane depends more on the growth orientation of the crystals than on the deposited crystal salt amount [25]. A characterization of the scaling and crystal structure could be carried out by membrane removal and further conditioning steps. For this purpose atomic absorption spectrometry (AAS), X-ray diffraction (XRD), grazing incidence wide angle X-ray scattering (GIWAXS), vertical scanning interferometry (VSI) and atomic force microscopy (AFM) are applied [25]. Also, some recent publications deal with the influences of scaling inhibiting or modifying ingredients as they occur in real applications. For example, it is recently shown by SEM and EDX that an optional upstream ultrafiltration resulted in an increased scaling caused by a reduction of organic matter [23]. An induction time theory at existing supersaturation is assumed since long for various scaling substances such as $CaCO_3$. However with regard to $CaCO_3$, it is now considered that the induction time theory is

https://doi.org/10.23763/BrSc23-03hager

Authors

Simon Hager*, Helge Oesinghaus*, Thomas Hofmann, Karl Glas, Water Systems Engineering, Chair of Food Chemistry and Molecular Sensory Science, TUM School of Life Sciences, Technische Universität München, Freising, Germany; Alexander Bachmann, Rainer Engelbrecht, Polymer Optical Fiber Application Center (POF AC), Technische Hochschule Nürnberg Georg Simon Ohm, Nuremberg, Germany; Martin Meinardus, Grünbeck Wasseraufbereitung GmbH, Höchstädt a.d. Donau, Germany; corresponding author: simon.hager@tum.de, helge.oesinghaus@tum.de, *these authors contributed equally to this work

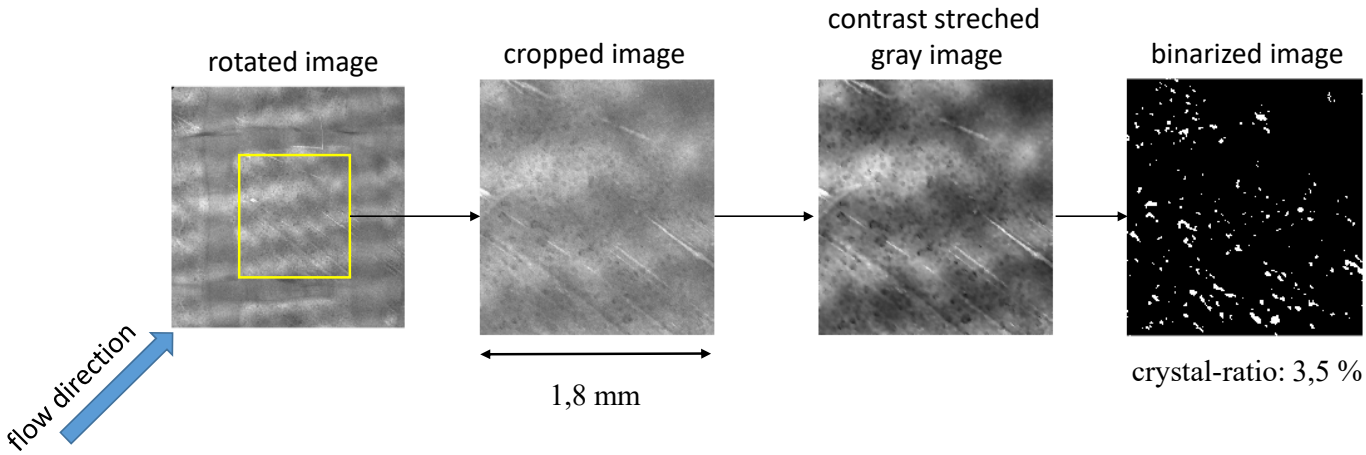

Fig. 1 **Image processing for crystal detection on the membrane surface. From left to right: Rotated image, taken in transmitted light mode, Cropped image, Contrast stretched grey scaled image, Final binarized image with detected crystals on the surface (white points) and the crystal-ratio = white pixels/total pixels**

not applicable and that only the late detectability in the membrane process had led to this assumption [12]. Nevertheless, the induction time theory is still used in scaling research on $CaCO_3$. For example, in their experiments, *Mangal* 2021 et al. defined the time span up to a pH drop of 0.03 units by $CaCO_3$ precipitation as the induction time [13]. For the evaluation of sulphate deposits such as $CaSO_4$, the induction time is frequently used in the recent literature [1–3, 9].

In general, the methods used for scaling analysis can be divided into ex-situ and in-situ analysis. The classical in-situ approaches of scaling detection by evaluation of membrane performance such as flux or permeability can only indicate advanced scaling. Using the ex-situ methods, the membrane modules used must be opened and are thereby destroyed to examine the suspected salt precipitation. The major advantage of ex-situ methods is the subsequent applicability in a great variety of analysis methods such as described above. However, when removing and handling membranes outside the membrane modules to examine the crystal structures, numerous possible influences must be considered. For example, influences on the crystalline structures by crystal ripening or a subsequent formation of crystals by evaporation and drying of dissolved salt residues on the membranes must be considered. In addition to the elaborate and mostly destructive ex-situ methods described here as examples, we have already given an overview of existing in-situ sensor systems in Part 1 of this publication series [6]. The need for a universal and simple detection method for early-stage scaling and fouling in general is pointed out there. This need for research and development of detection methods is also highlighted as an important research gap in recent literature [12]. The purpose of this paper is to demonstrate the potential of a new optoelectronic in-situ and highly sensitive detection method based on polymer optical fibres.

This is the third part of our publication series on $CaCO_3$ scaling in RO membrane modules. In Part 1, the state of the science on the prediction and detection of $CaCO_3$ scaling is presented. The results displayed in this work are based on a new measurement method using POF. This principle is presented in Part 1 and placed in comparison to current methods. In Part 2, a new hydrochemical simulation model is demonstrated, which is used in this paper as a basis for describing the saturation of important $CaCO_3$ polymorphs and crystallization zones.

2 Methods and Materials

This study aims at the combination of predictive calculations of $CaCO_3$ supersaturation on RO-membrane surfaces with several monitoring methods to detect deposits on RO membranes. To start, the monitoring methods among them the image analysis and the setup of polymer optical fibre sensors will be presented in the sections 2.1 and 2.2. In a second step saturation predictions and the experimental setups will be described.

2.1 Image analysis Method

The flat membrane module made of Polymethylmethacrylate (PMMA) allows to take pictures in transmitted light mode. The advantage is that $CaCO_3$-crystals scatter the light out of the optical line “light source-membrane-camera” (see Fig. 3) due to their deviating refractive index, such they appear dark in the photo. The pictures are taken with a Basler-acA3088-57uc CMOS camera every 5 minutes. The images can be focused on the membrane surface due to inhomogeneities on the surface.

Imaging of the membrane surface and subsequent image processing is aimed at detecting $CaCO_3$-crystals on the membrane surface. The recorded images are processed with MATLAB 2020b software. The detection of the crystals allows the determination of the membrane area covered with crystals.

Figure 1 illustrates the steps of image processing. The images are rotated and then cropped so that the free membrane area can be further analysed in a feed spacer square of 1.8 x 1.8 mm. The feed flows diagonally through the feed spacer square. Photos are typically described by three matrices with the red, green and blue components. The original colour RGB image is converted to a grey-scale image. To improve image quality, the contrast stretching method is often used [16]. Using this method, the crystals on the membrane surface become more visible. The membrane area

coated by crystals can be measured using binarization of the grey-scaled image. As a threshold to binarize the grey image a local adaptive function with a brighter background is employed. For binarization an adaptive method is used, such that brightness differences do not impact the image analysis. Finally, a crystallisation ratio was calculated by comparing the area ratios of the overall image to the area covered with crystals. The minimum size for the detection of the $CaCO_3$-crystals is a covered membrane area of 350 µm².

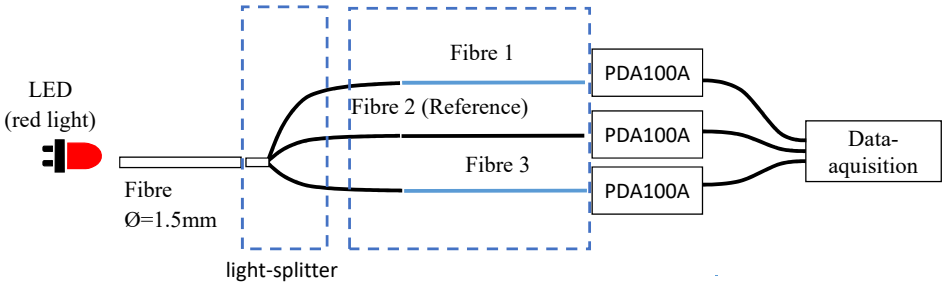

Fig. 2 Polymer optical fibre setup as a sensor for scaling detection

2.2 Optical fibre setup

We chose as fibres for the optical sensors Asahi Luminos DB 500 polymer optical fibres (POF) with a diameter of 500 µm. The fibre consists of a PMMA core and a fluoropolymer cladding. For the scaling detection, the 10 µm fluoropolymer cladding is removed as a sensor zone with a length of 5 cm using ethylacetate. This principle was already illustrated in the first part of this publication series [6]. In the sensor zone, the light rays interact with deposits on the fibre surface, because there is the possibility of interrupting the total reflection of the light in the fibre. In figure 2 these are the modified sensor-fibres 1 and 3.

As shown in figure 2, red light (656 nm) is emitted in a light splitter and into the POF for scaling detection. Red LED are commonly used for data communication over POF because of the low optical attenuation in this wavelength region [26]. Fibre 2 is the reference fibre without a sensor zone. This fibre is used to detect optical power fluctuations which are not due to scaling, for example due to thermally fluctuating LED power or detection sensitivity of the sensor, or due to ageing of LED, detectors and fibres. For measuring the optical power (optometry), the transmitted optical power of all fibres is detected by amplified photodetectors (Thorlabs PDA100a), and their output voltage U proportional to the optical power P is registered digitally. The optical setup is used in the RO flat cell as well as in water bath experiments, where supersaturated salt solutions with sulphates and $CaCO_3$ were examined.

For the data processing, only relative transmission signals τ are used. τ is calculated by the ratio between the measured transmitted light power P and the intrinsic transmitted power at the beginning of the experiments P_0. In addition, the behaviour of the reference fibre is included in the calculation of τ.

$$\tau = \frac{P}{P_0} - \frac{P(ref)}{P_0(ref)} + 1 \qquad \text{(Eq. 1)}$$

2.3 PHREEQC calculations

The measurement-based detection methods are compared with hydrochemical simulations performed using PHREEQC software – describing the supersaturation of $CaCO_3$ and sulphates. The calculation of $CaCO_3$ as ΔpH value is carried out as described in Part II of this publication series [8]. CO_2 passage through the membrane is calculated according to measured pH values in the retentate stream. The calculations were run in PHREEQC version 3.7.3.15968 using the phreec.dat database. Rising pH values in the feed solution with the second experimental protocol in section 3.2 are also adapted by CO_2 extraction. Saturations of sulphates for the water bath experiments are likewise calculated using the phreec.dat database.

2.4 Experimental setup – POFs in different supersaturated salt solutions

The primary purpose of the initial tests with the POF sensors is to prove the theoretically forecasted influence of crystallisation on the sensor signal. The secondary objective is to achieve different salt precipitations on the surfaces of the POF so that common scaling components could be tested.

Therefore, the POFs are installed in supersaturated salt solutions. The experiments are carried out in triplicate, with $CaSO_4$, $BaSO_4$, $SrSO_4$ and $CaCO_3$ being investigated. The $CaCO_3$ – solution is tested in pure form as well as with 2 different concentrations of the antiscalant MT4000. The experiments are carried out at a temperature of 21 °C. The pH value is measured with a pH-meter, type WTW Multi 3320. Table 1 lists the concentrations of all synthesised salt solutions

Table 1 Examined salt solutions with the individual components from which the crystals on the POF surfaces were formed

final desposit	solution 1	solution 2	saturation index	precipitate name	precipitation potential in mmoL/L
$CaCO_3$	99 mmol/l $NaHCO_3$	33 mmol/l $CaCl_2$	Calcite: 2.5 (1.4 as ΔpH) MCC: 1.2 (0.9 as ΔpH) ACC: 0.5 (0.4 as ΔpH)	Calcite	30
$CaSO_4$*$2H_2O$	70 mmol/l Na_2SO_4	70 mmol/l $CaCl_2$	0.7	Gypsum	46
$SrSO_4$	8.2 mmol/l Na_2SO_4	8.2 mmol/l $SrCl_2$	1.6	Celestite	7.5
$BaSO_4$	1.50 mmol/l Na_2SO_4	1.50 mmol/l $BaCl_2$	3.7	Barite	1.49

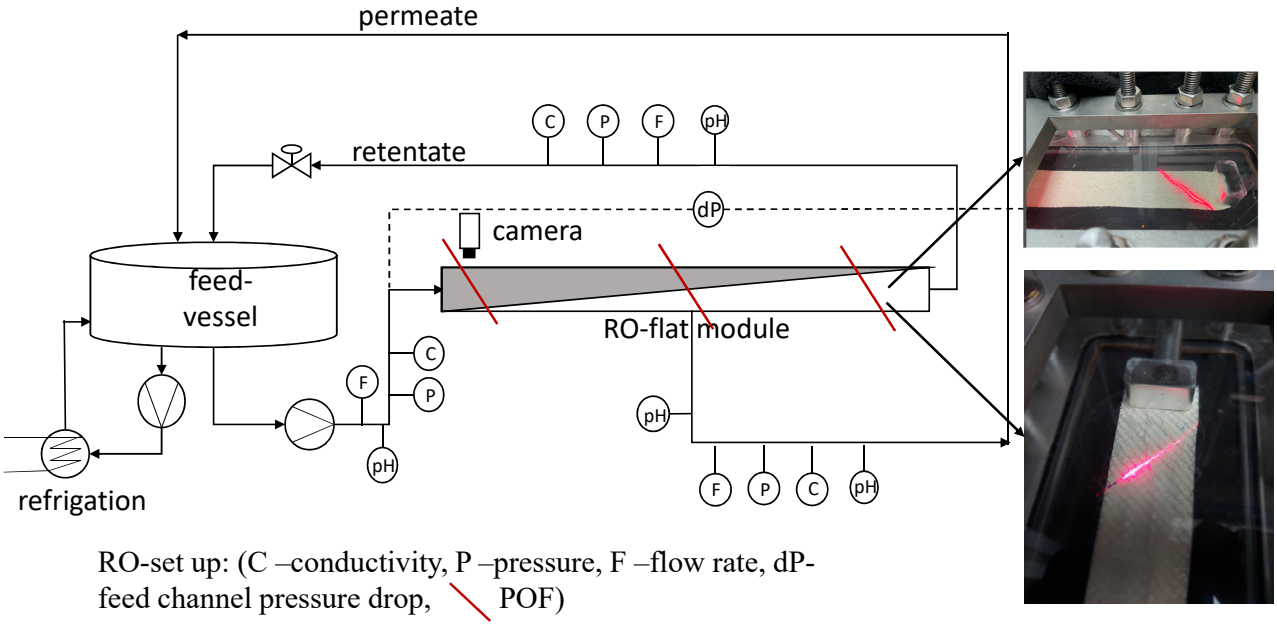

Fig. 3 Schematic diagram and photo of the RO pilot plant, involving a crossflow membrane flat module with POF sensors

together with the component salts which form the final deposit on the POF surface. Based on Gibbs free energy, the supersaturation, i.e. saturation indices greater than 0, represent a measure of the driving force of precipitation [6]. After the experiments, the POFs are dried, and pictures are taken of the POF surfaces with a light microscope.

2.5 Experimental RO-setup

The experiments to investigate the effects of scaling in an RO-filtration system are carried out in a crossflow filtration setup with a spacer-filled channel. A schematic diagram of the pilot-RO-system is provided in figure 3. The crossflow conditions are representative for spiral wound membrane modules [21]. Before the scaling experiments started, the hydraulics of the cell are validated by comparing the expected pressure drop and measured values with calculations according to *Schock* and *Miquel* (1987) [20]. By a variation of the cross-flow velocity, the pressure drop could be measured and compared to the theory [20].

For this study, thin film composite membranes (Type: DOW XLE) with a size of 95 cm x 3.4 cm ~ 300 cm² are used. The storage of the low-pressure membranes takes place in 4 % $Na_2S_2O_3$ at 20 °C until the experiment starts.

For all crystallisation experiments, synthetic water containing $NaHCO_3$ and $CaCl_2$ is mixed in an 80 l feed vessel. The concentrations and $CaCO_3$ saturations are shown in associated sections 3.2 and 3.3. The test solutions are prepared newly for each experiment and kept almost constant at 20 °C (± 1 °C) by cooling. The test solution is fed via a Novados H1 pump through the feed-sensor module (pH, conductivity, temperature, flow rate) in the flat membrane module.

In the feed channel above the membrane and under the feed spacer three POFs are diagonally installed along and between two fibres of the feed spacer. The pH value, the conductivity, and the flow rate of the permeate and retentate are measured continuously. Table 2 lists the sensor types used in the RO-pilot plant.

All sensor data is collected and stored by a Siemens S7 SPS in time intervals of 1-second. The retentate flow is automatically kept constant by a motorised needle valve and the flow rate sensor in the retentate, so that the crossflow velocity stays 10 cm/s during the tests. Such flow velocity and resulting Reynolds number are found in retentate side membrane modules in practice [8]. The feed pressure is automatically kept constant at 12 bar by coupling the pressure sensor in the feed and a frequency converter for the feed pressure pump. Further parameters are shown in table 3. They are determined in a reference experiment with 2000 ppm NaCl feed solution.

During the experiments, the supersaturation of the different polymorphs of $CaCO_3$ is reached by adjusting the concentration (reject permeate) or by dosing sodium hydroxide in the feed vessel to the solution containing Ca^{2+} and dissolved carbon. The experimental protocol and its results are presented in the following chapter.

Table 2 Sensor types in the RO-pilot plant

measurand	place	sensor type
flow rate	retentate	Endress und Hauser Promass A 300/8A3B01 DN 01
flow rate	permeate	Natec NU-140
conductivity	feed, retentate	Jesco-LF-110 (0-20mS/cm)
conductivity	permeate	Jesco-LF-110 (0-1mS/cm)
pH	feed, retentate, permeate	Hamilton Polylite-Plus-H-Arc-120
temperature	feed, permeate	PT-100- Jesco-LF-110
pressure	feed, retentate, permeate	Wika-A-10
differential pressure	feed-channel	Endress und Hauser Typ PMD75

Table 3 **RO Parameter measured in a reference experiment with 2000 ppm NaCl-feed-solution**

RO-parameter	Formula symbol	Magnitude
flux	J_W	55 L m^{-2}
recovery	r	30 %
temperature	T	20 °C ± 1 °C
concentration factor	CF	1.45
Reynolds number	Re	140
Schmidts number	Sc	800
Sherwoods number	Sh	2.5
concentration polarisation	β	1.1

3 Experimental Setups and Results

The series of experiments are splitted into three parts. Firstly, POFs are immersed in the supersaturated salt solutions. In the second part an experimental protocol is discussed in which the supersaturation of all $CaCO_3$-polymorphs in the RO-pilot plant is reached by continuous dosing NaOH to the feed-solution. The third experimental protocol is devoted to a constant feed concentration in analogy to the literature [14] in order to apply conditions that are as relevant to industrial practice as possible.

3.1 Experimental protocol – POF in highly supersaturated salt solutions

The first experimental protocol is a setup for POFs placed in supersaturated water solutions. The aim is to prove that different salt deposits on POF's surfaces cause a drop of light transmission. Is this hypothesis hold, the transmission drop means the detection of salt deposits via polymer optical fibre sensors.

Therefore, the POFs are tested in calcium carbonate, calcium sulphate, barium sulphate and strontium sulphate solutions. These are common deposits on RO-membrane surfaces. All solutions are supersaturated, see table 1. Figure 4 shows the course of the transmission for the sulphate solutions together with photos of the POF surfaces taken after the experiments, that is reached when a quasi-steady state of τ is reached.

The photos clearly show the crystals on the POF surfaces. The crystals have different morphologies such as the characteristic needles from gypsum. As the experiment progresses, the light transmission τ via the sensor fibres decreases. For all three sulphate salts τ drops in the first phase of the experiment. Later τ approaches an almost constant level.

In the present sulphate experiments, the saturation indices increase from $CaSO_4$ to $SrSO_4$ and finally to $BaSO_4$ (see Table 1). The precipitation kinetics determined with the POF also show this relationship with the fastest transmission decline in the $BaSO_4$ experiments. Note also that the slightly supersaturated $CaSO_4$ solution show a relatively slow transmission decline over several hours.

The following experiments show the detection of $CaCO_3$-crystals in water bath of the salt solutions. Also, the influence of antiscalant (AS) MT 4000 on the crystallisation and in particular on the development of transmission decline is shown. As a reference measurement for $CaCO_3$ precipitation, the development of the pH value is also monitored.

In all experiments $CaCO_3$-scaling is indicated by decreasing pH values as well as decreasing transmittance values of the POFs. Trigonal calcite deposits are visible on the fibre surfaces in the photos. With increasing concentration of the AS, the transmission decreases less. Furthermore, the increasing AS concentration delays the transmission loss.

The weaker decrease in transmission indicates decreasing crystallisation. 10 mg/L AS cause a delay of 2 – 5 minutes of the strong transmission drop at the beginning of the experiment. For the AS experiments, the photos show less but larger crystals. Commonly, AS impacts the free surface of crystal clusters, thereby retarding the formation rate and growth rates of crystallisation [18].

We conclude that, all salt precipitations ($CaSO_4$, $BaSO_4$, $SrSO_4$ and $CaCO_3$) cause a strong transmission loss via the POFs with a

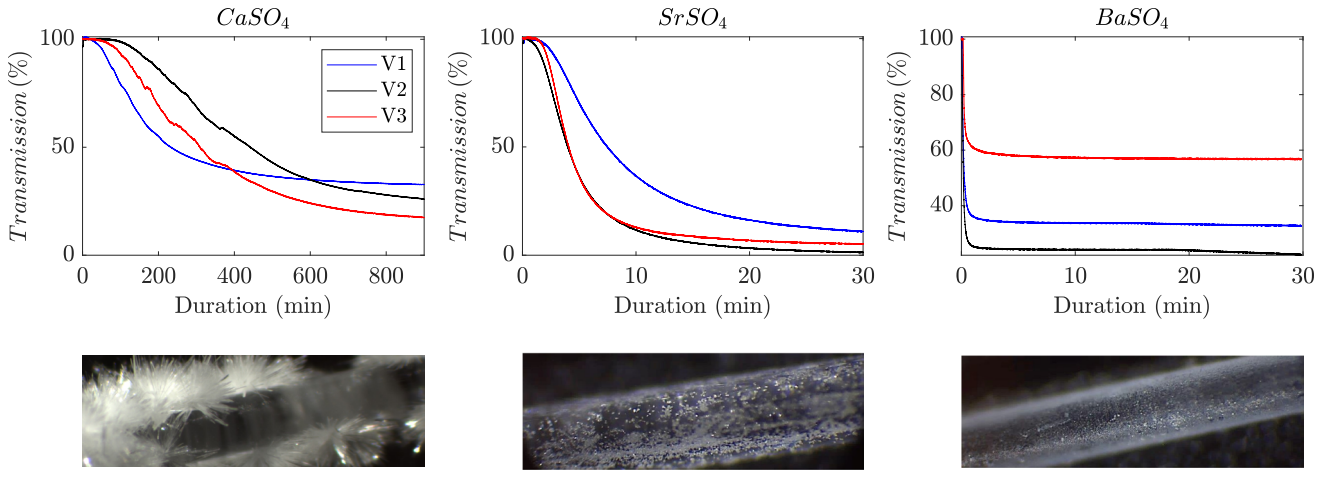

Fig. 4 **Upper part: Transmission data from the POFs immersed in the sulphate solutions. From left to right: Calcium sulphate, strontium sulphate and barium sulphate. Lower Part: Photos of the POFs after the experiments with respective salt crystals on their surfaces. V1, V2, V3 describe the triplicate**

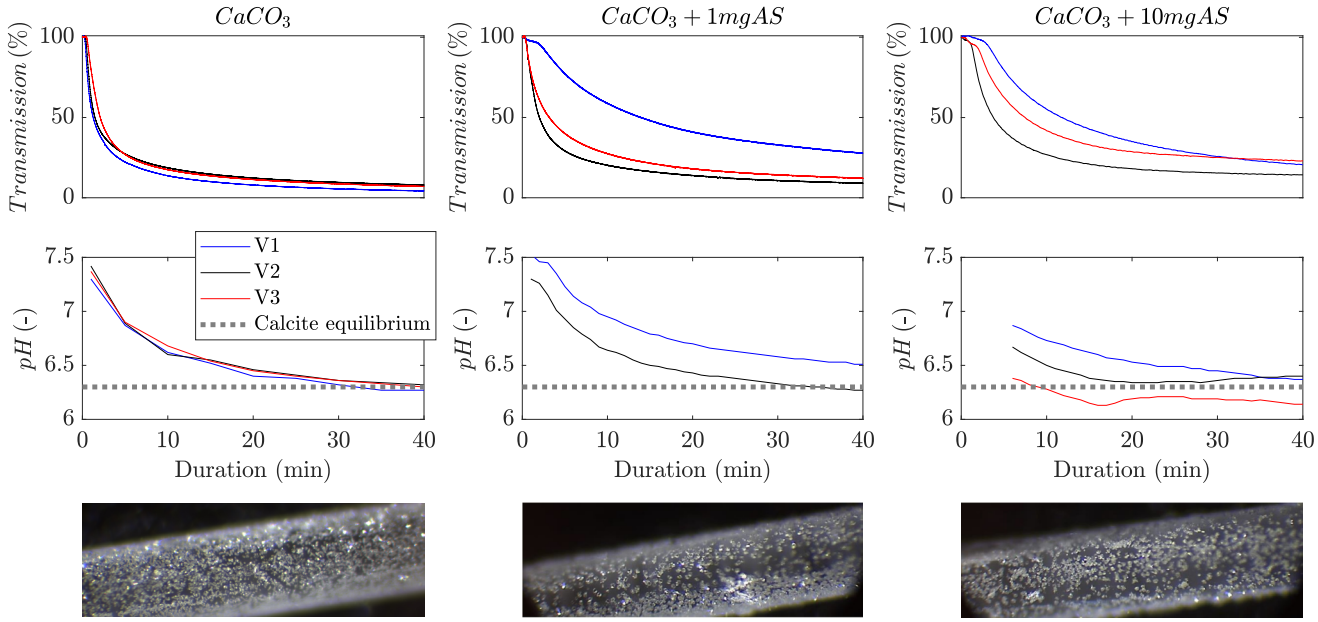

Fig. 5 **Experimental data from POFs immersed in $CaCO_3$-solutions. Top row: transmission data of POFs immersed in a pure $CaCO_3$-solution, a solution with 1 mg/l antiscalant (AS) MT4000 and 10 mg/l. Middle row: Development of the pH values of the corresponding experiments. Bottom Row: Photos of the POFs after the experiments with the salt crystals on their surfaces**

sensor zone. In combination with the AS, the transmission behaviour is changed and slowed down. These experiments proof that POFs can be a universal sensing element for precipitation detection of salts relevant in reverse osmosis technology.

3.2 Experimental protocol – membrane cell – supersaturating $CaCO_3$ via pH adjustment

In this section we start the experiments with undersaturated solutions for all $CaCO_3$-polymorphs. The experiments are designed so that undersaturation of all $CaCO_3$-polymorphs in the solution is achieved by the dosage of HCl down to pH = 4.5.

The experimental conditions, including the crossflow velocity v = 10 cm/s and the feed pressure p_{feed} = 12 bar, are kept constant during

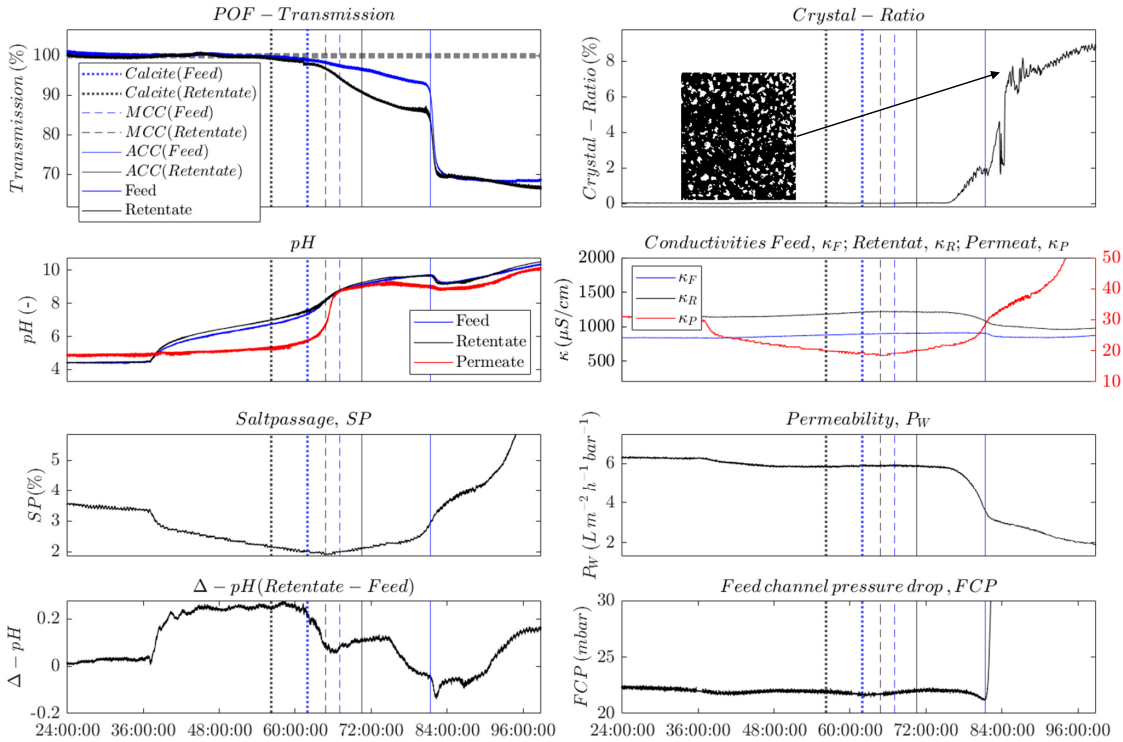

Fig. 6 **Time series from the experiment with $CaCO_3$- supersaturating via pH adjustment. The initial pH value is adjusted with hydrochloric acid to 4.5. Then the supersaturation of the $CaCO_3$-polymorphs is achieved by dosing 0.1M NaOH into the feed water. The vertical lines mark the first occurrence of supersaturation of the $CaCO_3$-polymorphs in the feed and the retentate**

the whole experiment. The experiment is obtained in full-recycle mode.

The saturations values of all polymorphs were determined with the software PHREEQC.

Each experimental protocol is run in triplicate. They are started with cleaning the RO-system using citric acid at pH = 3. Next, the rinsed membrane with feed-spacer, permeate-spacer and three POFs are installed in the membrane flat cell. Among the POFs, one fibre is a reference-fibre where the cladding is intact; hence no detection of deposits is possible by this fibre. The POFs with sensor zones were included on the feed side of the flat cell and the retentate side.

The experimental procedure includes first a conditioning phase for 12 h at experimental conditions but with desalinated tap water. After the conditioning phase, 2 mMol/l $CaCl_2$; 3.5 mMol\l $NaHCO_3$ and 3.2 mMol/l HCl are mixed in the feed vessel. Each salt is pre-solved in 5 l desalinated water and then mixed in 80 l desalinated water. This procedure avoids homogenous crystallisation. The undersaturated $CaCO_3$-solution is then pumped through the RO-system for a period of 24 hours in complete recycling mode. Then the dosing of 10 ml/h 0.1 M NaOH is started at experimental time = 36 h until the pH value of 11 is reached as the end of the experiment. During the entire experiment, photos are taken every 5 min with a resolution of 3088 x 2064 pixels. After the termination of the experiments (i.e. 144 h), the membranes and the POFs were dried and prepared for light- and scanning electron microscopy.

The experimental data of one experiment are shown in figure 6. The two remaining experiments of the triplicate show similar results.

The total experimental duration is 144 h. The time series show the effects of crystallisation in the RO-plant until 96 h for closer visualisation of the most relevant period. The FCP value increased by about 300 % at the very end. The FCP serves a measure for hydraulic resistance along the membrane, and is therefore indicating a narrowing of the flow channel along the membrane at the constant volume flow rate. Note that the salt passage first decreases, and later increases. The early decrease is caused by the pH-dependent salt rejection of polyamide-RO-membranes [22]. The following increase indicates scaling. The salt passage increases by about 750 % throughout the whole experiment. The water permeability through the membrane is decreasing by about 80 %. All these basic parameters indicate the $CaCO_3$-crystallisation and deposition in the RO-system. The conductivities in the feed and retentate remain almost constant until strong crystallisation occurs at time = 80 h.

Figure 6 also shows the time series of the calculated crystallisation rate which is shown in more detail in figure 7 (image processing see section 2.1).

Until 72 h no crystals on the membrane surface are detected. From 82 h forward the crystal-ratio increases strongly. After 75 h a slight increase of the crystal ratio can be observed.

During this first increase the $CaCO_3$- crystals are rather located in the lower left corner of the processed image. Due to the location of the first visible crystals, the $CaCO_3$-crystals seem to be formed and grow in the flow shadows behind the feed-spacer (see Fig. 1). This indicates a higher concentration polarisation (CP) in flow-shadowed regions on the membrane surface. CP often calculated as a mean value describing a whole membrane module. In fact, it is known that the flow conditions in spacer filled feed channels are widely inhomogeneous [24]. The local flow conditions influence the local CP directly [4].

Another effect illustrated in figure 7 is the plateau of the crystal-ratio as reached after the first detected crystals (t = 84 h). Even when the membrane surface is fully covered with $CaCO_3$-crystals the crystal-ratio will never reach the value of 100 %. This discrepancy may be caused by inevitable approximation in image processing when dealing with overlapping crystals. These overlapping crystals cause a backscattering of the transmitted light into the optical line “light source-membrane-camera”, so that the crystals appear no longer dark in the captured images and are no longer detectable. This effect can be proofed by SEM analysis as shown in figure 8. This picture illustrates the overlapping calcite crystals on the membrane surface.

In conclusion, the image analysis method can give a good impression of the first visually detected $CaCO_3$-crystals and of the

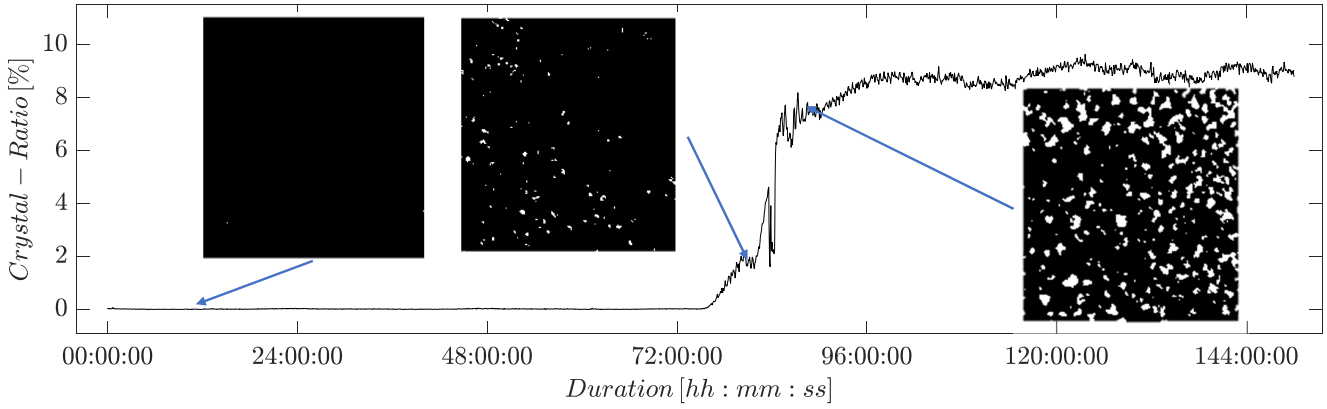

Fig. 7 Crystal-RatioTime series with raw images and binarized images. From left to right: no Scaling; light Scaling; progressed scaled Membrane

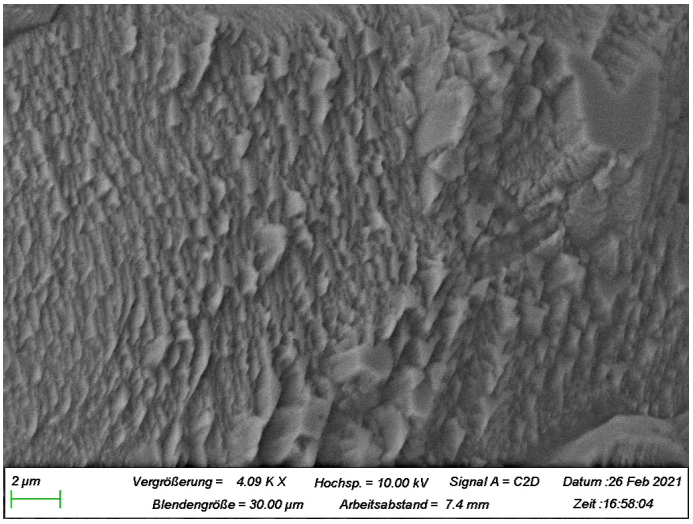

Fig. 8 SEM picture of overlapping calcite crystals on the RO membrane surface. The picture is taken after an experiment with increasing pH value

incipient crystallisation. However, as the crystallisation proceeds, overlapping crystals make a correct calculation of crystallisation ratio impossible. A realistic view of the crystallisation on the membrane surface can be obtained between the plateau, where the crystals overlap each other and the first crystals are detected; this holds for t = 75 h until t = 84 h in the experiment shown in figure 7.

In RO-plants, heterogeneous crystallisation is to be expected the predominate crystallisation pathway (undersaturation of ACC). A major challenge during the experiments is to reproduce heterogeneous crystal nucleation in the RO-pilot plant. There are two theories for the crystal formation in the literature. According to the theory of *Karabelas* et al. (2013) heterogeneous crystallisation takes place whenever calcite is supersaturated [14]. They proved their theory by SEM imaging of crystal nuclei formation on RO-membrane surfaces. *Elfil* et al. (2006) purpose a heterogeneous crystallisation as soon as monohydrated $CaCO_3$ (MCC) is supersaturated [5]. MCC is the precursor for crystal nuclei formation.

Our experiments, presented in this paper with initial undersaturated start, the theory of Elfil et al. (2006) seems more suitable since simultaneously to the saturation of MCC we observe an alteration in the salt passage and also the transmitted light through the POFs.

The ΔpH in figure 6 indicates the difference in pH values between feed and retentate stream. It also changes with the supersaturation of calcite in the feed solution. The pH value in the retentate increases in this time range by 0.2 compared to the pH value in the feed. Precipitation of $CaCO_3$ leads to decreasing pH values and could therefore indicate precipitation in the membrane cell. This interpretation again is rather compatible to Karabelas theory (2013) [14].

Three parameters feed channel pressure drop, permeability, and the calculated image crystal-ratio are changing simultaneously to the supersaturation of amorphous $CaCO_3$ (ACC). This indicates

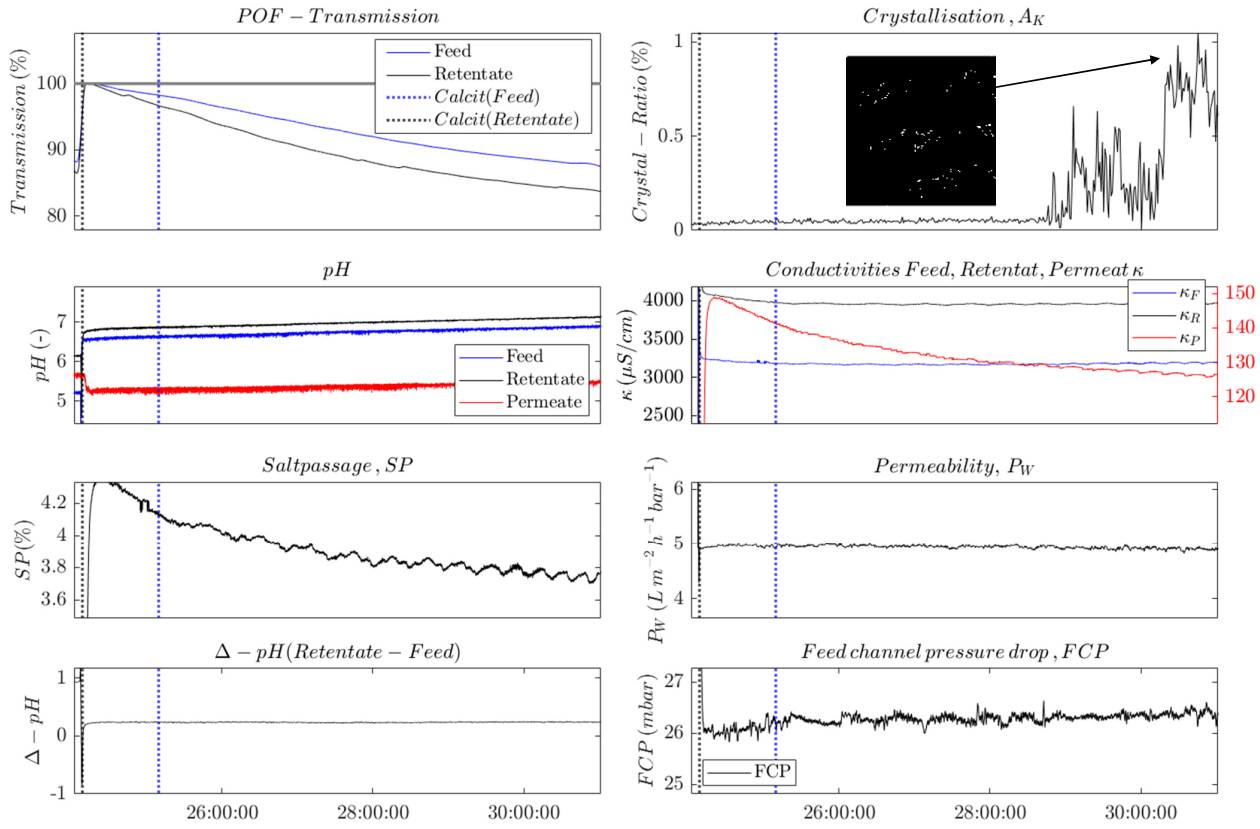

Fig. 9 Time series of an experiment with calcite supersaturation in the retentate stream. The compaction phase of the membrane lasted up to 24 hours. Then the experiment is continued with almost constant saturation conditions where calcite is supersaturated. The pH value is adjusted to 6.8 with HCl at the beginning of the experiment. The vertical lines mark the first occurrence of supersaturation of calcite in the feed and the retentate. MCC and ACC are undersaturated during the experiment

the expected strong homogenous crystallisation in the RO-plant according to the theory of Elfil et al. (2006) [5]. With the saturation of ACC, the POF signal also reacts strongly with a rapid decrease of light transmission. The transmission loss at this point is much stronger as it is at the saturation point of MCC previously.

In summary, the calculation for the $CaCO_3$ saturation of different polymorphs (vertical lines in Fig. 6) are a good indicator of when precipitation on the membrane surface is to be expected. The POF sensor is sensitive to incipient crystallisation on the membrane surface. Incipient crystallisation is detected by the first transmission drops earlier than the common parameters permeability, FCP or even image analysis. The salt passage changes in time with the POF transmission drops. However, it is unclear whether this is due to scaling alone or to the pH-dependent behaviour of the salt passage.

Certainly, it is difficult to distinguish between primary or secondary crystallisation. The RO-pilot system is not designed and built according to the principles of hygienic design. Therefore, incomplete cleaning of crystal residues is possible, which may lead to secondary crystallisation from the beginning of each experiment. However, the second and strong transmission loss of the POF sensors (ACC saturation in the feed water) indicates that the pH increases during the experiment initially led to primary, heterogeneous crystal formation in the feed channel. Our saturation calculations on MCC and ACC saturation support this hypothesis.

The presented experimental results in this section do not allow a clear preference to either the theory of Karabelas et al. (2013) [14] or the theory of precursor role of MCC of Elfil et al. (2006) [5]. In order to produce heterogeneous scaling on the membrane with greater reliability, another experimental setup is performed in the RO-pilot plant.

3.3 Experimental protocol – membrane cell – constant conductivities and pH values

In the third experimental protocol, presented in this section, the saturation is kept almost constant. This leads to a more realistic RO-setup. The functionality of the POF sensor can thus be examined for practice-orientated precipitate formation. Firstly, a compaction phase proceeded for 24 h. Secondly, the feed solution is mixed in the feed vessel. The feed solution consists of 11.8 mMol/l $CaCl_2$ and 6.5 mMol/l $NaHCO_3$. The pH value is adjusted to 6.8 by HCl. The experimental protocol includes a discharge of permeate and retentate during the experiment. The whole experimental setup is as close as possible to that of *Mitrouli* and Karabelas et al. (2013, 2016) [14, 15]. They propounded the theory that no induction time exists and $CaCO_3$ precipitates immediately after supersaturation of calcite. Figure 9 presents our experimental results.

The calcite is supersaturated in the retentate since the beginning of the experiment after the compaction phase. Calcite saturation in the feed is reached at duration = 25 h due to a slight shift in pH value likely due to CO_2 degassing from the ventilated circulation tank. The experimental data show the effect of light scaling in the RO-system. The permeability is slightly decreasing from 5 to 4.9 L h^{-1} bar^{-1} m^{-2}, and the pressure drop in the feed channel is increasing slowly from 26.0 to 26.5 bar. The origin of these marginal trends, which stand out only slightly from the signal noise, cannot be clearly determined. The salt passage is decreasing by 15 %. This might be an effect of a post-compaction of the membrane during the experiment. The image analysis is the only parameter that shows that crystallisation is certainly taking place in the RO-system. From 29 h time forward, small crystals are detected by the image analysis. The level of crystallisation detected in the images is only 1 %. This means that the crystal-ratio calculated by automatically image analysis is below the above-mentioned plateau level, where the overlapping crystals affect the image analysis. Regarding to the minimum detection level of 350 µm² for each crystal the image analysis gives a realistic view of emerging $CaCO_3$ crystals on the membrane surface.

The light transmission through the POFs is immediately decreasing after dosing the salts in the feed vessel. As in section 3.2. the retentate fibre transmission is decreasing stronger than the feed fibre transmission. This can be explained by an earlier and stronger crystallisation on the retentate side of the membrane cell. Here, the salt concentration and thus the supersaturation is higher than in feed side of the cell. As shown in figure 9 scaling is detected earlier and more strongly by the POF sensors than any other parameter in the reverse osmosis system.

The SEM-picture in figure 10 illustrates the effect of POF on RO-membrane surfaces. Clearly visible are the crystals formed near and beneath the POF. It appears as if the POF is partially embedded in the crystals. Furthermore, the crystals are mainly growing near to the POF imprint on the membrane surface. This could be explained due to high local salt saturation, which is enhanced by a higher concentration polarisation in the flow shadows generated by the POFs. Hence, the crystals grow firstly in the area around the POFs and in consequence the functioning of the POF as an early scaling sensor seems positively influenced by this locally enhanced concentration polarization as it also appears at the feed spacer fibres along the membrane channel.

In addition, the SEM image (Fig. 10) shows a membrane surface not completely covered with crystals. As explained above, the im-

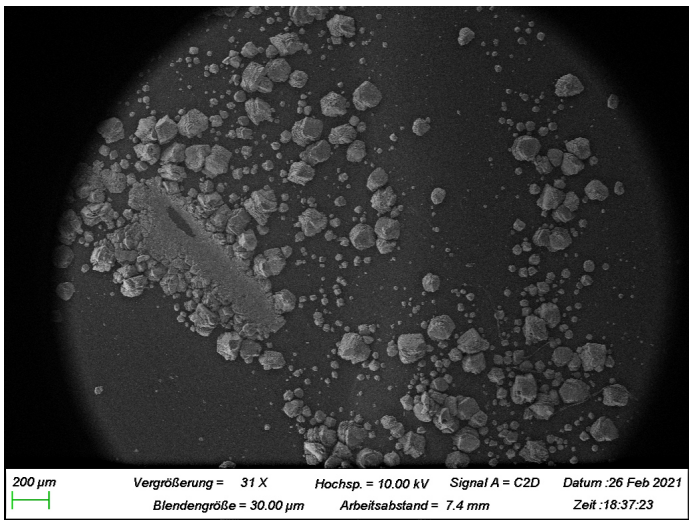

Fig. 10 SEM Picture with a POF imprint from an experiment with constant conductivities and pH values

age processing can therefore still detect single crystals. The time series given in figure 9 have not reached the plateau value of 10 %, which is known from the experiments described in 3.2.

In conclusion, the comparison of our experiments with those of Karabelas et al. (2016) led to similar results [14]. After the triplicate, it can be stated that the supersaturation of calcite is sufficient for crystal growth on RO-membrane surfaces. This has been demonstrated using online sensors such as the POF sensors and image analysis, as well as the offline method through SEM analysis. The results show that supersaturation prediction of MCC is not necessarily the key factor for the critical formation of crystals. It cannot be finally determined whether this is due to an early primary crystal formation or due to crystal nuclei remaining in the RO-system after rinsing with citric acid, which cause secondary crystal growth.

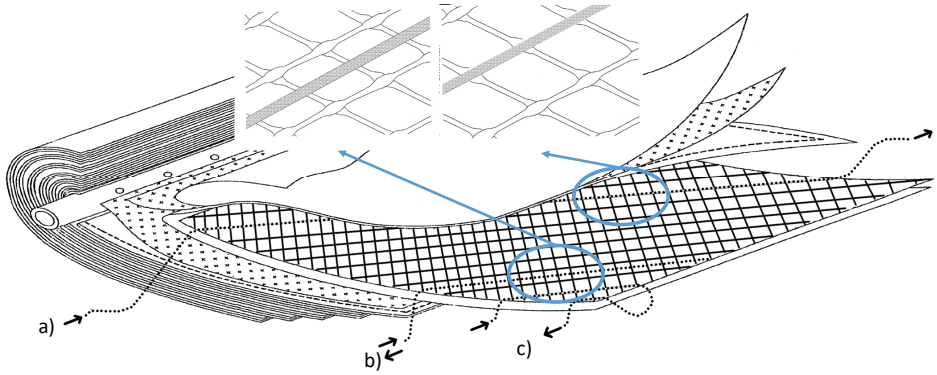

Fig. 11 Integration concept for polymer optical fibres in spiral wound RO-modules: a) POF is replacing a feed-spacer fibre, b) POF with a mirror on the fibre end, c) back and forth integrated POF in the feed-spacer [7]

4 Conclusion

In this study, two new in-situ methods for the scaling detection in RO-modules are presented:

1. An early detection of inorganic precipitations on the RO-membrane surface and in vitro is possible by using polymer optical fibre (POF) sensors. This leads to a method by which crystallisation processes in RO-systems can be detected before the crystallisation itself impacts on the performance of the RO-filtration. It is proofed in two experimental designs (each executed in triplicate), that in the very moment when the POF first detects crystals the performance of the RO-system is not deteriorate. The membrane permeability (i.e. normalised water flux) and the salt rejection decrease later in the experiments. The feed-channel pressure drop does not increase or increases only many hours after the POFs already have detected the crystals on the membrane. The sensitivity of the POF sensor is proofed in an RO-flat membrane cell with $CaCO_3$ and in water solutions with $CaSO_4$, $BaSO_4$, $SrSO_4$ and $CaCO_3$ in combinations with an antiscalant.

2. The second in-situ monitoring method for crystallisation processes in membrane flat modules is an image analysis method for the detection of the crystals and for the assessment of their sizes. Due to this method in combination with the transparent PMMA-membrane flat cell we were able to detect $CaCO_3$-crystals with a covered membrane area of 350 µm². The image analysis detects crystallisation processes earlier than the membrane performance begins to decrease. This is proved in the experiments guided by the experimental setup of Karabelas and Mitrouli et al. (2020, 2013) [12][14]. The image analysis method is suitable to validate the presented POF sensors. The POFs can now also be used with spirally wound membrane modules where the image analysis method does not work.

The accompanying simulation methods (published in Part I and II) for calculating saturation by the pH value in the salt solution allows to predict precipitation in experiments. These simulation methods support the functionality of the POFs. The $CaCO_3$ polymorphs calcite, MCC and ACC were simulated. By our experiments it could not be clarified beyond doubt whether MCC plays a precursor role as in the experiments of Elfil et al (2006) [5]. As has already been shown in the literature with laboratory-scale experiments [12][14], it is doubtful whether induction time or meta stability [5] play a role in $CaCO_3$ crystal formation in such experimental set-ups.

5 Outlook

This chapter gives an overview of integration concepts for the new POF sensor in industrial-scale RO systems [7]. On the one hand, it is possible to couple flat membrane cells with POF as a monitoring device to such full-scale systems. In addition, figure 11 shows various possibilities for integrating POF into spiral-wound modules. Concepts a) and c) must be included during the production of spiral wound modules. Replacing a spacer fibre by a POF has the advantage of avoiding additional flow shadows in the feed channel. This is desirable since the local concentration polarisation may be enhanced by additional fibres in the spacer net.

Another strategy for integrating the POF sensor into conventional spiral-wound modules is shown with concept b). Here, a POF sensor with a front-side mirror (e.g. gold coating) is inserted between two membrane sheets. A realistic approach is to use POF sensors to detect incipient crystal nuclei in the last spiral wound module where the salt concentrations reach the highest values. For the detection of biological fouling the approach of Vrouwenvelder et al. [24] seems more suitable. The highest nutrient loads and therefore biofouling is found in the membrane modules on the feed side. Therefore, a feed-side module should be equipped with a POF sensor for biofouling detection.

Acknowledgements

The authors wish to thank Heribert Voit (Endress + Hauser) for the suitable cooperation and the rental of sensors to execute the experiments.

6 References

1. Abdel-Ghafar, H. M.; Abdel-Aal, E. A. and El Anadouli, B. E.: Study on the nucleation aspects and morphology of reverse osmosis desalination scales with and without scale inhibitor at different supersaturation ratios, Water Supply, **17** (2017), no. 2, pp. 493-499.
2. Benecke, J.: Gypsum scaling during reverse osmosis desalination – characterization and effects of natural organic matter, TUHH Universitätsbibliothek, 2018.
3. Bystrianský, M.; Nir, O.; Šír, M.; Honzajková, Z.; Vurm, R.; Hrychová, P.; Bervic, A. and van der Bruggen, B.: The presence of ferric iron promotes calcium sulphate scaling in reverse osmosis processes, Desalination, **393** (2016), pp. 115-119.
4. Crittenden, J. C.: MWH's water treatment: Principles and design, John Wiley and Sons, Hoboken, N.J., 2012.
5. Elfil, H. and Hannachi, A.: Reconsidering water scaling tendency assessment, AIChE J., **52** (2006), no. 10, pp. 3583-3591.
6. Hager, S.; Bachmann, A.; Hofmann, T.; Engelbrecht, R. and Glas, K.: $CaCO_3$ deposits in reverse osmosis Part I - Shortcomings of current approaches leading to a new prediction model and monitoring device, BrewingScience, **74** (2021), no. 9/10, pp. 122-133.
7. Hager, S. and Glas, K.: Membranmodul und Verfahren zur Detektion von Ablagerungen in einem Membranmodul, WO002018192945A1.
8. Hager, S.; Meinardus, M.; Hofmann T. and Glas, K.: $CaCO_3$ deposits in reverse osmosis: Part II - Simulation model for hydrochemical predictions of reverse osmosis retentates and scaling propensity, BrewingScience, **75** (2022), no. 7/8, pp. 54-68.
9. Jaramillo, H.; Boo, C.; Hashmi, S. M. and Elimelech, M.: Zwitterionic coating on thin-film composite membranes to delay gypsum scaling in reverse osmosis, Journal of Membrane Science, **618** (2021), p. 118568.
10. Jiang, S.; Li, Y. and Ladewig, B. P.: A review of reverse osmosis membrane fouling and control strategies, The Science of the total environment, **595** (2017), pp. 567-583.
11. Jiang, W.; Xu, X.; Johnson, D.; Lin, L.; Wang, H. and Xu, P.: Effectiveness and mechanisms of electromagnetic field on reverse osmosis membrane scaling control during brackish groundwater desalination, Separation and Purification Technology, **280** (2022), no. 1-2, p. 119823.
12. Karabelas, A. J.; Mitrouli, S. T. and Kostoglou, M.: Scaling in reverse osmosis desalination plants: A perspective focusing on development of comprehensive simulation tools, Desalination, **474** (2020), p. 114193.
13. Mangal, M. N.; Salinas-Rodriguez, S. G.; Blankert, B.; Yangali-Quintanilla, V. A.; Schippers, J. C.; van der Meer, W. G. and Kennedy, M. D.: Role of phosphate and humic substances in controlling calcium carbonate scaling in a groundwater reverse osmosis system, Journal of Environmental Chemical Engineering, **9** (2021), no. 4, p. 105651.
14. Mitrouli, S.; Karabelas, A. J.; Karanasiou, A. and Kostoglou, M.: Incipient calcium carbonate scaling of desalination membranes in narrow channels with spacers – experimental insights, Journal of Membrane Science, **425-426** (2013), pp. 48-57.
15. Mitrouli, S. T.; Kostoglou, M. and Karabelas, A. J.: Calcium carbonate scaling of desalination membranes: Assessment of scaling parameters from dead-end filtration experiments, Journal of Membrane Science, **510** (2016), pp. 293-305.
16. Negi, S. S. and Bhandari, Y. S.: A hybrid approach to Image Enhancement using Contrast Stretching on Image Sharpening and the analysis of various cases arising using histogram. In International Conference on Recent Advances and Innovations in Engineering (ICRAIE-2014), IEEE, 1–6, DOI=10.1109/ICRAIE.2014.6909232, 2014.
17. Pervov, A. G.: Scale formation prognosis and cleaning procedure schedules in reverse osmosis systems operation, Desalination, **83** (1991), no. 1-3, pp. 77-118.
18. Popov, K.; Oshchepkov, M.; Pervov, A.; Golovesov, V.; Ryabova, A.; Trukhina, M. and Tkachenko, S.: A Case Study of Calcium Carbonate Crystallization during Reverse Osmosis Water Desalination in Presence of Novel Fluorescent-Tagged Antiscalants, Membranes, **12** (2022), no. 2, p. 194.
19. Sarker, N. R.; Cherukupally, P.; Gourevich, I.; Wilbur, J.; Jons, S. D. and Bilton, A. M.: Multi-scale visualization of incipient CaCO3 scaling on the polyamide layer of reverse osmosis membranes, Desalination, **539** (2022), p. 115956.
20. Schock, G. and Miquel, A.: Mass transfer and pressure loss in spiral wound modules, Desalination, **64** (1987), pp. 339-352.
21. Siebdrath, N.; Ding, W.; Pietsch, E.; Kruithof, J.; Uhl, W. and Vrouwenvelder, J.: Construction and validation of a long-channel membrane test cell for representative monitoring of performance and characterization of fouling over the length of spiral-wound membrane modules, DWT, **89** (2017), pp. 1-16.
22. Stolov, M. and Freger, V.: Membrane Charge Weakly Affects Ion Transport in Reverse Osmosis. Environ. Sci. Technol. Lett., **7** (2020), no. 6, pp. 440-445.
23. Tong, X.; Zhang, Z.-W.; Wu, Y.-H.; Bai, Y.; Ikuno, N.; Ishii, K. and Hu, H.-Y.: Ultrafiltration significantly increased the scaling potential of municipal secondary effluent on reverse osmosis membranes, Water research, **220** (2022), p. 118672.
24. Vrouwenvelder, J. S.; Kruithof, J. C. and van Loosdrecht, M. C. M.: Biofouling of spiral wound membrane systems, IWA Publishing, London, 2011.
25. Wang, M.; Cao, B.; Hu, Y. and Rodrigues, D. F.: Mineral Scaling on Reverse Osmosis Membranes: Role of Mass, Orientation, and Crystallinity on Permeability, Environ. Sci. Technol., **55** (2021), no. 23, pp. 16110-16119.
26. Ziemann, O.; Krauser, J.; Zamzow, P. E. and Daum, W.: POF-Handbuch. Optische Kurzstrecken-Übertragungssysteme. Springer, Berlin, Heidelberg, 2007.

Received 31 January 2023, accepted 17 February 2023